Novel Magnetic Polymer/bentonite Composite: Characterization and Application for Re(VII) and W(VI) Adsorption

Bojana M. Marković[1*)], Ivan S. Stefanović[1], Aleksandra B. Nastasović[1], Zvjezdana P. Sandić[2], Ljiljana T. Suručić[3], Aleksandra Dapčević[4], Jasna V. Džunuzović[1], Zvonko Jagličić[5], Zorica M. Vuković[1], Vladimir Pavlović[6], Antonije E. Onjia[4]

[1]University of Belgrade – Institute of Chemistry, Technology and Metallurgy, Njegoševa 12, Belgrade, Serbia
[2]University of Banja Luka, Faculty of Natural Science and Mathematics, Mladena Stojanovića 2, Banja Luka, Republic of Srpska, B&H
[3]University of Banja Luka, Faculty of Medicine, Save Mrkalja 14, Banja Luka, Republic of Srpska, B&H
[4]University of Belgrade, Faculty of Technology and Metallurgy, Karnegijeva 4, Belgrade, Serbia
[5]University of Ljubljana, Faculty of Civil and Geodetic Engineering & Institute of Mathematics, Physics and Mechanics, Jamova 2, Ljubljana, Slovenia.
[6]University of Belgrade, Faculty of Agriculture, Nemanjina 6, Zemun, Serbia

Abstract:

A novel magnetic polymer/bentonite composite was prepared by suspension copolymerization of glycidyl methacrylate and ethylene glycol dimethacrylate in the presence of magnetic bentonite (MB-PGME) and functionalized with ethylene diamine and hexamethylene diamine (MB-PGME-ED and MB-PGME-HD). The obtained samples were characterized in terms of structure as well as thermal, magnetic and morphological properties. The sorption of rhenium (Re) and tungsten (W) from aqueous solution onto MB-PGME-ED and MB-PGME-HD was investigated considering their contact time and different initial ion concentration, giving possibility for usage of these composites as commercial sorbents. The sorption system follows the pseudo-second order and intraparticle diffusion kinetic models. The results indicated a better fit with the Freundlich isotherm model.
Keywords: Glycidyl methacrylate; Magnetic bentonite; Amino-functionalization; Sorption.

1. Introduction

Bentonite clay is a low-cost alumina-silicate clay mineral having a unique sandwich structure, good chemical and mechanical stability. Due to its large specific surface, high sorption affinity, and cation exchange capacity [1,2], bentonite is widely used in the removal of many toxic metal ions, like Cu(II), Co(II), Cd(II), Ni(II), Pb(II), Fe(II) and Zn(II), from aqueous solutions [3-5]. On the other hand, the separation of fine bentonite particles from aqueous solution after adsorption of metal ions is difficult. To overcome this, the magnetic

_____

*) **Corresponding author:** bojana.markovic@ihtm.bg.ac.rs

_____

polymer/clay nanocomposites that combine the structure, physical, and chemical properties of both inorganic and organic materials are needed. Combining bentonite with a magnetic amino-functionalized copolymer of glycidyl methacrylate (GMA) and ethylene glycol dimethacrylate (EGDMA), MB-PGME, could be an effective route to improve bentonite properties because hydroxyl (-OH) and amino groups ($-NH_2$) in amino-functionalized PGME can serve as the active sites for binding with heavy metals [6]. In addition, amino and hydroxyl groups of each GMA unit may form hydrogen bonds with the silicate hydroxylated end groups (AOH) and SiAOASi groups of bentonite, leading to the strong interaction between amino-functionalized copolymer and bentonite [7].

Rhenium (Re) and tungsten (W) are indispensable in modern industries. Rhenium is used in oil refinery industries and high-temperature superalloys [8,9]. Tungsten, due to its excellent high-temperature mechanical properties and the fact that it can easily be processed, cannot be substituted in different fields of modern technology, like electronics, aerospace components, drilling equipment, etc. [10]. Because of the strong need for these metals, there is a growing interest in the removal and recovery of rhenium and tungsten from industrial wastewaters.

To our knowledge, there are no published studies related to the use of magnetic PGME/bentonite composite as Re(VII) and W(VI) sorbent. In this work, the amino-functionalized composites of magnetic bentonite and macroporous GMA and EGDMA (MB-PGME) were tested as a potential Re(VII) and W(VI) sorbents from aqueous solutions.

2. Materials and Experimental Procedures

The preparation of MB-PGME-ED and MB-PGME-HD is presented in Scheme 1. Firstly, the magnetic bentonite nanoparticles were synthesized via coprecipitation of $FeCl_2·4H_2O$ (VWR International) and $FeCl_3·6H_2O$ (VWR International) in the presence of bentonite (Sigma-Aldrich), as reported in the literature [11] and designated as MB. Then, magnetic composite (MB-PGME) was prepared by *in-situ* suspension copolymerization of GMA (Merck) and EGDMA (Sigma-Aldrich) in the presence of inert component and 10 wt.% MB nanoparticles [12]. Finally, a fraction of beads MB-PGME with diameters d<0.1 mm was functionalized with ethylene diamine (ED, Sigma-Aldrich) (MB-PGME/ED ratio was 1/2.5 (w/w)) and hexamethylenediamine (HD, Sigma-Aldrich) (MB-PGME/HD ratio was 1/5 (w/w)) [12]. The samples were labeled as MB-PGME-ED and MB-PGME-HD.

The morphology of the obtained samples was observed by SEM (JEOL JSM-6460LV) and TEM (JEM–1400 Plus). The samples were coated with gold in a high-vacuum evaporator prior to the SEM analysis. The TEM was operated with the acceleration voltage of 120 kV and a $LaB6$ filament. The functional groups in the samples were determined in ATR mode using FTIR spectroscopy (Nicolet 380). Pore size distributions in samples were determined by mercury porosimetry (Porosimeter 2000; software Milestone 200). Thermal degradation of the synthesized samples was investigated by TGA (SDT Q600 analyzer) in N_2 atmosphere (flow rate: 100 cm^3/min; heating rate: 20 °C/min), from room temperature to 700 °C. Magnetic measurements were carried out by a SQUID magnetometer (MPMS XL-5). Hysteresis loops were measured at 300 K in the applied DC fields up to 5 T. A Philips PW 1050 X-ray powder diffractometer with Cu $K\alpha$ radiation ($\lambda = 1.5418$ Å) was used for the X-ray diffraction (XRD) analysis.

All sorption experiments were performed in batch static conditions at pH 7.6 and room temperature (298 K) with the same volume of Re(VII) and W(VI) aqueous solutions (V=20 cm^3) and MB-PGME-ED or MB-PGME-HD mass of 0.2 g. Metal stock solutions were prepared by dissolving reagent grade of $Na_2WO_4·×2H_2O$ (Acros Organic) and $NaReO_4$ (Sigma-Aldrich) in groundwater from Bukulja mountain near Aranđelovac (Serbia). The

_____

effect of contact time (0 – 180 min) and the initial Re(VII) or W(VI) concentration (10 – 90 mg/L) was studied. After sorption, sample aliquots were withdrawn, and analyzed with ICP-OES (iCAP6500). All the sorption experiments were conducted in triplicate. The sorption capacity Q_t (mg/g) at time t was calculated with the following equation:

$$Q_t = \frac{(C_i - C_t)V}{W} \qquad (1)$$

where C_i (mg/L) and C_t (mg/L) are the initial concentration and the concentration at the time t of Re(VII) and W(VI) in aqueous solution, respectively.
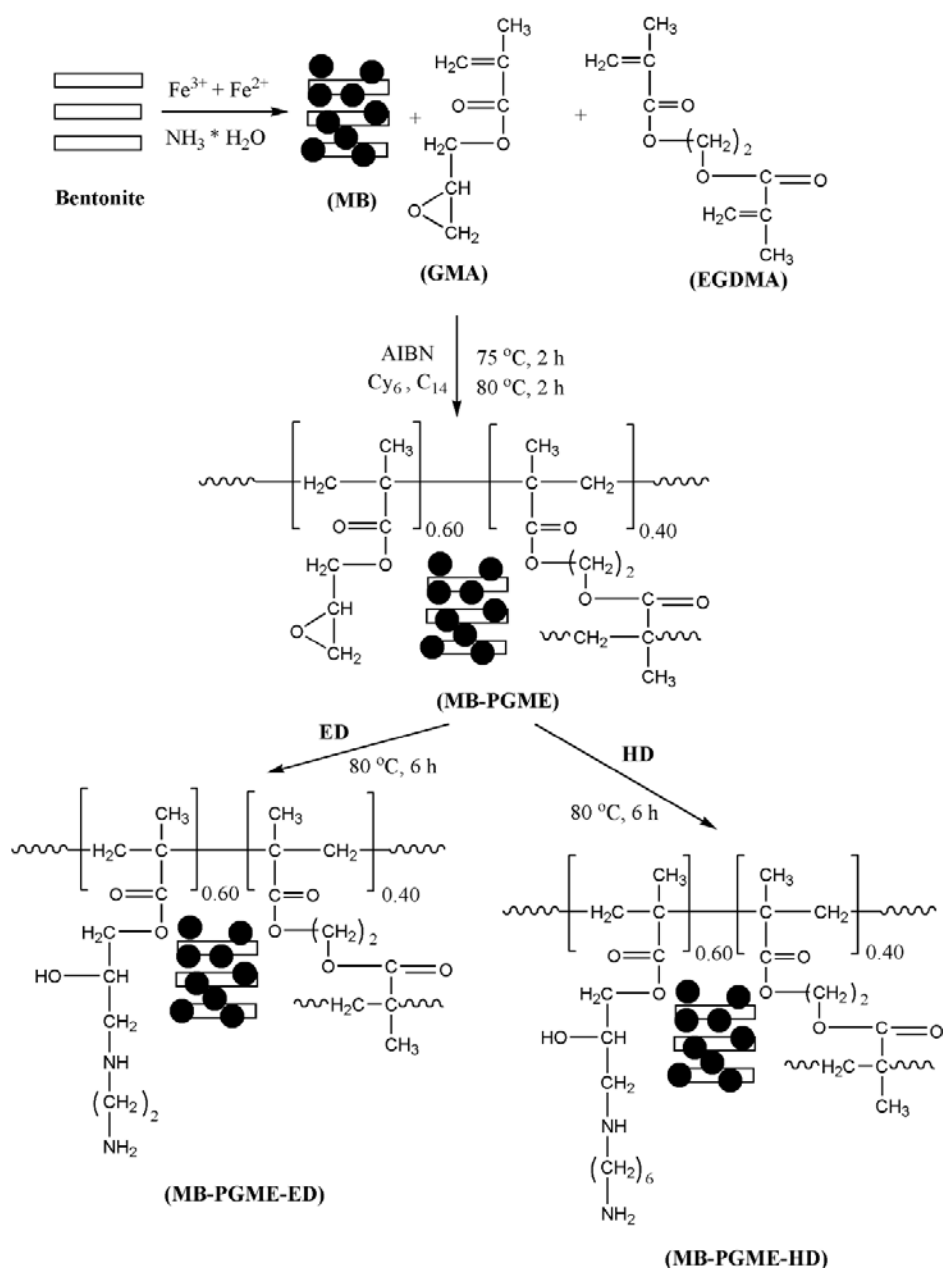
**Scheme 1.** Preparation of MB-PGME-ED and MB-PGME-HD sorbents.

_____

3. Results and Discussion

According to the SEM image (Fig. 1a), MB nanoparticles with irregular morphology are stacks of multi-layers with a sheet structure and embedded magnetite particles. As can be seen from the TEM image (Fig. 1b), the MB nanoparticles in a size range of 6 to 35 nm were synthesized. MB-PGME composite has the shape of regular, spherical particles (d < 0.1 mm) (given as inset in Fig. 1c), having three-dimensional porous structure clearly visible at particle cross-section (Fig. 1c). Mercury porosimetry shows a macroporous structure of MB-PGME with a specific pore area of 65 m^2/g and pore diameter which corresponds to the half of the pore volume of 87 nm. TEM image of MB-PGME (Fig. 1d) confirmed successful integration between the MB nanoparticles (dark) and amorphous macroporous copolymer (gray). Also, the dispersion of nano-clay particles (filament-like regions) in the composite with intercalation structure can be seen in Fig. 1d (indicated by an arrow). A similar result was reported in the literature [13].
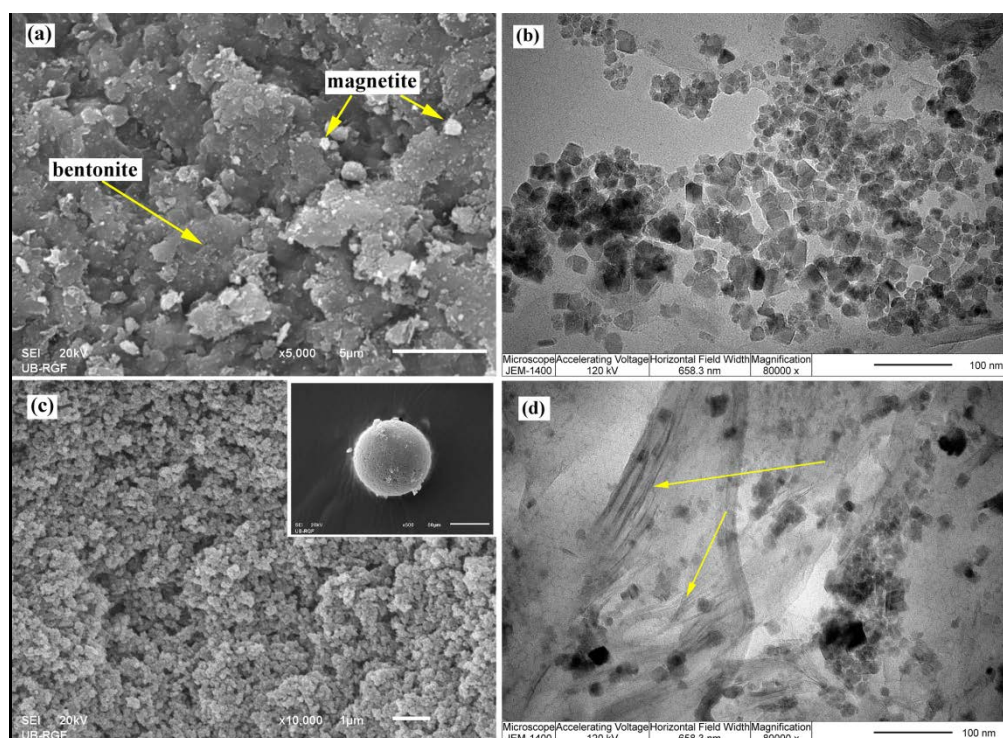
Fig.1. SEM microphotograph (a) and TEM image (b) of MB nanoparticles, SEM microphotographs of the cross-section and particle (inset) (c) and TEM image (d) of MB-PGME copolymer.

The absorption band at 3740 cm^{-1} (Fig. 2a) is due to the stretching vibration of the free silanol groups [14]. The bands at 3350 cm^{-1} and 1650 cm^{-1} could be ascribed to the stretching and bending –OH vibrations of the water molecules adsorbed on the bentonite/magnetite surface. The peak at 1400 cm^{-1} corresponds to the deformation vibrations of the –OH groups at the edges of the SiO_4 tetrahedra. A sharp band at 1045 cm^{-1} is attributed to the stretching vibrations of the Si–O–Si group [14, 15]. The band at 400-700 cm^{-1} confirms the Fe–O bond [12], while the band at 466 cm^{-1} is attributed to the deformation vibrations of the Si–O–Si group [16]. Although weak, bands characteristic for MB are visible in the MB-PGME spectrum, which confirms the incorporation of MB nanoparticles in the polymer matrix. Characteristic bands for copolymer matrix are also present [12].
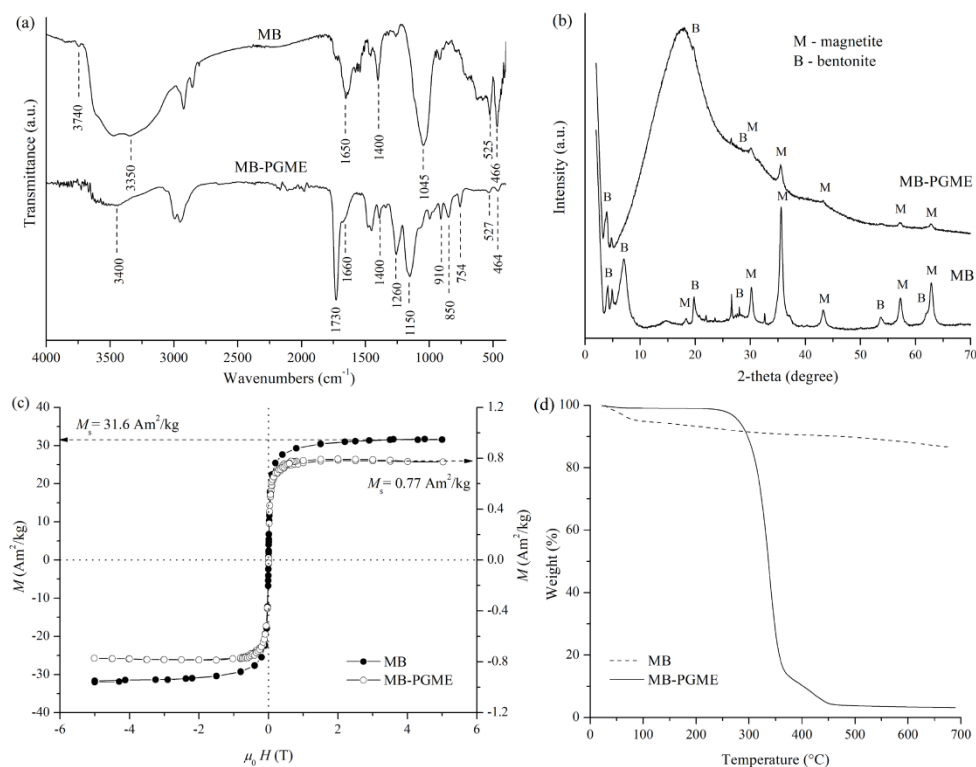
Fig. 2. ATR-FTIR spectra (a), XRD pattern (b), isothermal magnetization curves at 300 K (c) and TGA plots (d) of MB and MB-PGME samples.

The analysis of XRD patterns of MB and MB-PGME (Fig. 2b) confirmed the existence of magnetite in the MB and MB-PGME sample. Namely, the peaks at $2\theta = 30.2^o$, 35.4^o, 43.1^o, 57.2^o and 62.3^o are assigned to the (220), (311), (400), (511) and (440) reflections of cubic Fe_3O_4, respectively [11]. Also, the peaks at $2\theta = 4.8^o$ and 26.6^o, which are attributed to the montmorillonite and quartz in bentonite, respectively, confirmed the existence of bentonite in analyzed samples [11,17]. XRD pattern of MB-PGME also displays three humps in the region between 10°–25°, 25°–35° and 35°–40°, which could be attributed to the amorphous nature of PGME copolymer [18].

The remnant magnetization and coercivity of samples MB and MB-PGME (Fig. 2c) were very low, meaning that the resulting magnetic materials could be considered as superparamagnetic at 300 K. The values of saturation magnetization, M_s, of synthesized MB and composite MB-PGME were 31.6 Am^2/kg and 0.77 Am^2/kg, respectively. Comparison of the saturation magnetization values for MB-PGME and MB indicates that the content of MB nanoparticles in MB-PGME is 2.4 wt. %. The decrease in saturation magnetization of MB-PGME is the result of low concentrations of magnetic MB nanoparticles with respect to the non-magnetic polymer matrix.

The thermal decomposition curves of MB and MB-PGME are shown in Fig. 2d. TGA curve of MB show the weight loss between room temperature and 700 ^{o}C of about 13 wt.% that mainly could be related to the adsorbed water and decomposition of clay. The thermal decomposition of MB-PGME involves two degradation steps. The first step in the range of 200-350 ^{o}C could be associated with the decomposition of the random chain end, while the second step between 350 and 450 ^{o}C represents the total degradation of MB-PGME by random chain scission [19]. The TGA residue of approximately 3 wt.% observed for MB-PGME correlates well with MB content of 2.4 wt.% calculated from magnetization measurements.

_____

The morphology of surface and cross-section of amino-functionalized samples MB-PGME-ED and MB-PGME-HD are presented in Fig. 3a and Fig. 3b, respectively. It can be observed that the porous structure remains preserved after functionalization. However, no significant changes were observed in the specific surface area of functionalized samples MB-PGME-ED (68 m^2/g) and MB-PGME-HD (70 m^2/g) relative to the initial sample MB-PGME (65 m^2/g), as well as in the pore diameter, which corresponds to half of the pore volume (97 nm for MB-PGME-ED and 95 nm for MB-PGME-HD *vs*. 87 nm for MB-PGME).

The broad absorption band in ATR-FTIR spectra of MB-PGME-ED and MB-PGME-HD (Fig. 3c) with a peak at 3400 cm^{-1} corresponds to the overlapping of –OH and N−H stretching vibrations. The band at 1570 cm^{-1} and shoulder at ~1660 cm^{-1} could be ascribed to the bending of N–H and NH_2 vibrations [19]. The above results confirm the successful amino-functionalization of MB-PGME copolymer.
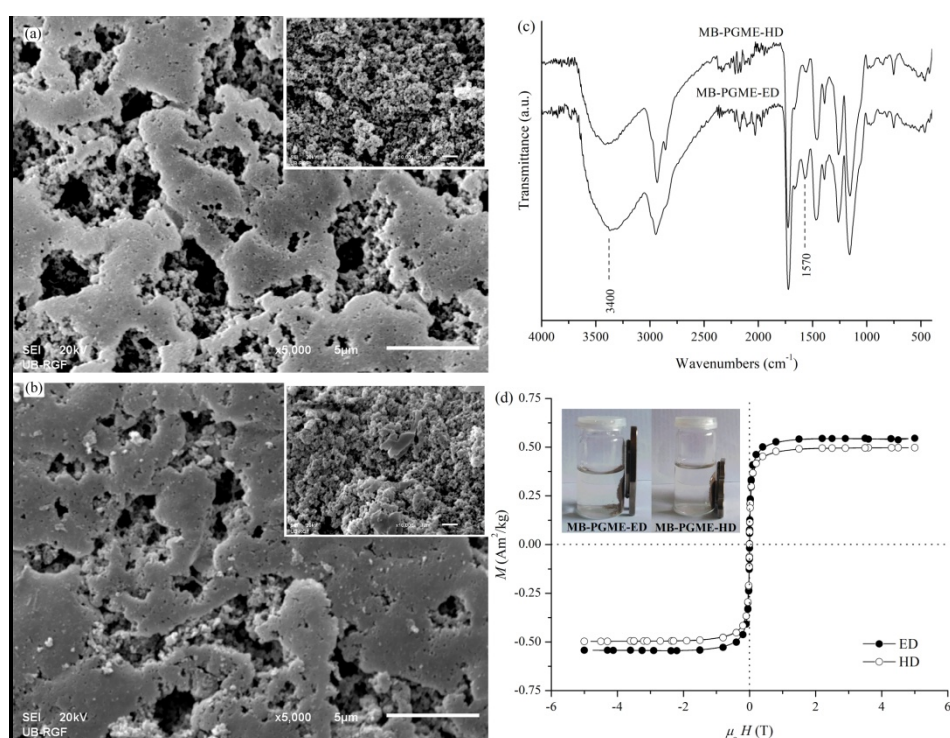

Fig. 3. SEM microphotograph of the surface and the cross-section (inset) of MB-PGME-ED (a) and MB-PGME-HD (b), ATR-FTIR spectra (c) and isothermal magnetization curves at 300 K (d) of MB-PGME-ED and MB-PGME-HD samples.

The magnetization measurements show that both amino-functionalized samples have preserved superparamagnetic behavior with a negligible hysteresis loop (Fig. 3d). The values of saturation magnetization (0.54 Am^2/kg and 0.50 Am^2/kg for MB-PGME-ED and MB-PGME-HD, respectively) are somewhat lower in comparison with the value obtained for the initial sample MB-PGME (0.77 Am^2/kg). The obtained results indicate that the values of magnetization saturation for amino-functionalized composites are high enough to separate MB-PGME-ED and MB-PGME-HD from aqueous solutions (Fig. 3d inset).

Due to their satisfying textural and magnetic properties, MB-PGME-ED and MB-PGME-HD were further tested as Re(VII) and W(VI) sorbents from aqueous solutions.

Fig. 4 demonstrates the results regarding the influence of contact time on Re(VII) and W(VI) sorption by MB-PGME-ED and MB-PGME-HD. It can be noticed that Re (VII) and W(VI) sorptivity was rapid in the first sorption phase, and then slowly increased over time.

Moreover, equilibrium sorption was observed only for Re(VII) and W(VI) onto MB-PGME-HD. Also, the amount of the sorbed ions was larger when MB-PGME-ED was applied.
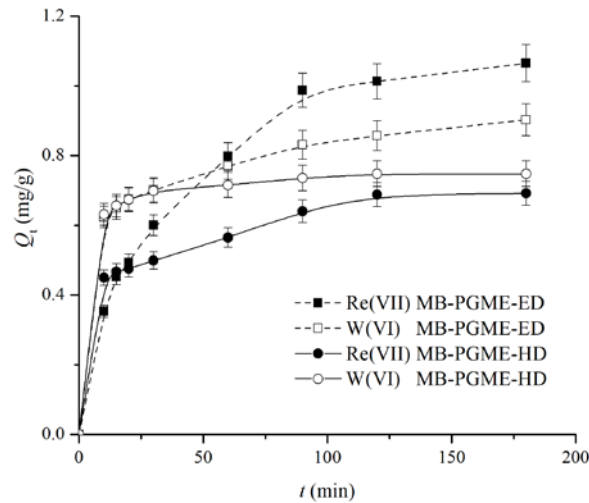
Fig.4. Effect of contact time on Re(VII) and W(VI) sorption from aqueous solutions onto MB-PGME-ED and MB-PGME-HD sorbents.

The pseudo-first order (PFO), the pseudo-second order (PSO) and intraparticle diffusion (IPD) kinetic models were employed to fit the sorption rate data of Re(VII) and W(VI) sorption onto MB-PGME-ED and MB-PGME-HD [20]. The relevant kinetic model parameters and correlation coefficients are given in Table I.

Tab. I The parameters of pseudo-first order, pseudo-second order and intraparticle diffusion models for sorption of Re(VII) and W(VI) onto MB-PGME-ED and MB-PGME-HD.

	MB-PGME-ED		MB-PGME-HD	
	Re(VII)	W(VI)	Re(VII)	W(VI)
Q_e^{exp} (mg/g)	1.06	0.90	0.69	0.75
Pseudo-first order model				
$k_1 \cdot 10^3$ (1/min)	23.03	16.12	32.29	25.33
Q_e^{calc} (mg/g)	0.94	0.33	0.46	0.13
R^2	0.980	0.996	0.861	0.973
Pseudo-second order model				
$k_2 \cdot 10^3$ (g/mg min)	28.35	131.12	125.68	519.31
Q_e^{calc} (mg/g)	1.24	0.93	0.73	0.76
R^2	0.996	0.998	0.996	0.999
Intraparticle diffusion model				
k_{1id}, (mg/g min$^{0.5}$)	0.097	0.032	0.025	0.029
$C_{1id} \cdot 10^2$ (mg/g)	6.07	52.56	36.70	54.10
R^2	0.997	0.997	0.990	0.992
k_{2id} (mg/(g min$^{0.5}$))	0.020	0.018	0.038	0.009
C_{2id} (mg/g)	0.80	0.66	0.279	0.65
R^2	0.998	0.999	0.993	0.993

k_1 – pseudo-first order rate constant (1/min), k_2 – pseudo-second order rate constant (g/ (mg min)), Q_e^{exp} – experimentally obtained value for amount of sorbed ions at equilibrium (mg/g), Q_e^{calc} – calculated value for amount of sorbed ions at equilibrium, k_{id} – intraparticle diffusion coefficient (mg/(g min$^{0.5}$)), C_{id} – constant, related to the thickness of the boundary layer (mg/g) and R^2 – correlation coefficients.

_____

The Q_e values calculated from PSO kinetic model for MB-PGME-HD are closer to the experimental Q_e values with higher correlation coefficients ($R^2>0.99$) than for the PFO model. The same can be observed for MB-PGME-ED. Besides, values of the Q_e calculated for MB-PGME-ED are somewhat higher than the highest determined values of the Q_t (1.06 mg/g for Re(VII) and 0.90 mg/g for W(VI)), which is in a good agreement with the results presented in Fig. 4. Therefore, the sorption process follows PSO kinetic model and the Re(VII) and W(VI) sorption goes faster when MB-PGME-HD is applied. Also, it is observed that IPD plots for both sorbents have two linear portions with high R^2 values (Table I), which indicated that the sorption is intraparticle diffusion controlled.

For the analysis of equilibrium data of Re(VII) and W(VI) adsorption Langmuir, Freundlich, Temkin and Dubinin–Radushkevich (D–R) isotherm models were used [21]. Calculated parameters from all isotherm models are listed in Table II.

Tab. II The parameters of Langmuir, Freundlich, Temkin and Dubinin–Raduskevich models for sorption of Re(VII) and W(VI) onto MB-PGME-ED and MB-PGME-HD from aqueous solutions.

	MB-PGME-ED		MB-PGME-HD	
	Re(VII)	W(VI)	Re(VII)	W(VI)
Langmuir				
Q_{max} (mg/g)	16.7	15.4	18.9	15.6
K_L (L/mg)	0.0256	0.0173	0.268	0.0130
R^2	0.866	0.798	0.851	0.846
Freundlich				
K_F ($L^n mg^{1-n}$/ g)	0.442	0.318	0.516	0.239
n	1.17	1.21	1.16	1.17
R^2	0.991	0.999	0.993	0.997
Temkin				
K_T (L/mg)	0.830	0.587	0.944	0.466
b_T, (kJ/mol)	1.25	1.47	1.18	1.54
R^2	0.926	0.876	0.923	0.901
Dubinin-Radushkevich				
K_D (mol^2/kJ)	1.05	1.59	0.864	2.37
Q_D (mg/g)	4.67	3.67	4.90	3.41
E (kJ/mol)	0.69	0.56	0.76	0.46
R^2	0.876	0.843	0.878	0.846

Q_{max} – Langmuir maximum adsorption capacity (mg/g), K_L – Langmuir isotherm constant (L/mg), K_F – Freundlich constant ($L^n mg^{1-n}$ /g), n – Freundlich isotherm exponent, K_T – Tempkin isotherm equilibrium binding constant (L/mg), b_T – Temkin isotherm constant (mg/L), Q_{DR} – D–R maximum adsorption capacity (mg/g) and K_D – D–R constant (mol^2/kJ^2).

The calculated monolayer saturation capacities according to Langmuir adsorption isotherm model for Re(VII) and W(VI) on MB-PGME-ED are 16.7 mg/g and 15.4 mg/g, respectively, while the Q_{max} values for Re(VII) and W(VI) on MB-PGME-HD are 18.9 mg/g and 15.6 mg/g, respectively. Also, the values of the dimensionless constant called the separation factor, R_L, were calculated (Eq.2) [22].

$$R_L = \frac{1}{1+K_L C_o} \qquad (2)$$

The R_L values are between 0 and 1 indicating favorable absorption of Re(VII) and W(VI) on both sorbents [22]. The average R^2 values indicate the best correlation of the equilibrium data with the Freundlich isotherm, followed by the D-R and Temkin, and then the Langmuir isotherm. These results suggest that the surface of MB-PGME-ED and MB-PGME-HD is

_____

heterogeneous and the adsorption of Re(VII) and W(VI) on both adsorbents is multilayer. The n values from the Freundlich equation were between 1.16 and 1.21, also indicating beneficial adsorption (Table II).

$$E = \frac{1}{\sqrt{2K_{DR}}} \qquad (3)$$

The mean energy of adsorption, E, (J/mol) (Eq. 3) calculated from D-R adsorption isotherm was used to estimate the mechanism of surface adsorption. The calculated E values (Table 2) are much lower than 8 kJ/mol, indicating that sorption of Re(VII) and W(VI) onto both sorbents is essentially physical in nature [23].

4. Conclusion

This study described the preparation, characterization and application of two amino-functionalized magnetic polymer/bentonite nanocomposites synthesized by suspension copolymerization. XRD analysis confirmed the existence of magnetite and bentonite in the MB-PGME, while ATR-FTIR spectra of MB-PGME-ED and MB-PGME-HD indicated that the amino groups were successfully grafted onto the surface of MB-PGME. The magnetization measurements showed a superparamagnetic behavior for both sorbents which are easily separated by an external magnetic field from aqueous solutions. Kinetic analysis indicated that sorption obeys PSO kinetic model, with a definite influence of pore diffusion. Freundlich model is the most appropriate for the Re(VII) and W(VI) sorption on MB-PGME-ED and MB-PGME-HD.

Acknowledgments

5. References

1.   A. Terzić, L. Pezo, Lj. Miličić, N. Mijatović, Z. Radojević, D. Radulović, Lj. Andrić, Sci. Sinter., 51 (2019) 39-56.
2.   A. Terzić, N. Đorđević, M. Mitrić, S. Marković, K. Đorđević, V.B. Pavlović, Sci. Sinter., 49 (2017) 23-37.
3.   J. G. Meneguin, G.R. Luz, I.C. Ostroski, M.A.S.D. de Barros, M.L. Gimenes, Chem. Eng. Trans., 24 (2011) 787-792.
4.   H. H. El-Maghrabi, S. Mikhail, J. Environ. Earth Sci., 4 (2014) 38-47.
5.   S. Mnasri-Ghnimi, N. Frini-Srasra, Appl. Clay Sci., 179 (2019) 105151.
6.   B. Podkościelna, J. Appl. Polym. Sci., 120 (2011) 3020-3026.
7.   Q. Liu, B. Yang, L. Zhang, R. Huang, Korean J. Chem. Eng., 32 (2015) 1314-1322.
8.   Z. Lou, C. Guo, X. Feng, S. Zhang, Z. Xing, W. Shan, Y. Xiong, Hydrometallurgy., 157 (2015) 199-206.
9.   L. Ye, Z. Ouyang, Y. Chen, S. Liu, Int. J. Refract. Met. Hard Mater., 87 (2020) 105148.
10.   G. Lefèvre, J. Lion, A. Makolana, Sep. Sci. Technol., 54 (2019) 549-558.

_____

11.   Z. Lou, Z. Zhou, W. Zhang, X. Zhang, X. Hu, P. Liu, H. Zhang, J. Taiwan. Inst. Chem. Eng., 49 (2015) 199-205.
12.   B. M. Marković, Z. M. Vuković, V. V. Spasojević, V. B. Kusigerski, V. B. Pavlović, A. E. Onjia, A. B. Nastasović, J. Alloys Compd., 705 (2017) 38-50.
13.   H. R. Nafchi, M. Abdouss, S. K. Najafi, R. M. Gargari, M. Mazhar, Maderas. Cienc. Tecnol., 17 (2015) 45-54.
14.   O. V. Alekseeva, A. N. Rodionova, A. V. Noskov, A. V. Agafonov, Clays Clay Miner., 67 (2019) 471-480.
15.   S. Stojiljković, M. Stamenković, D. Kostić, M. Miljković, B. Arsić, I. Savić, I. Savić, Sci. Sinter., 47 (2015) 51-59.
16.   M. Kokunešoski, M. Stanković, M. Vuković, J. Majstorović, Đ. Šaponjić, S. Ilić, A. Šaponjić, Sci. Sinter., 52 (2020) 339-348.
17.   I. S. Stefanović, M. Špírková, S. Ostojić, P. Stefanov, V.B. Pavlović, M. V. Pergal, Appl. Clay Sci., 149 (2017) 136-146.
18.   M. Imperiyka, A. Ahmad, S.A. Hanifah, M.Y.A. Rahman, Int. J. Polym. Sci., 2014 (2014) 638279.
19.   B. M. Marković, V. V. Spasojević, A. Dapčević, Z. M. Vuković, V. B. Pavlović, D. V. Randjelović, A. B. Nastasović, Hem. Ind., 73 (2019) 25-35.
20.   S. Marinović, M. Ajduković, N. Jović-Jovičić, P. Banković, Z. Mojović, A. Milutinović-Nikolić, D. Jovanović, Sci. Sinter., 48 (2016) 167-176.
21.   K. Trivunac, Lj. M. Kljajević, S. Nenadović, J. Gulicovski, M. Mirković, B. Babić, S. Stevanović, Sci. Sinter., 48 (2016) 209-220.
22.   S. S. Stupar, M. M. Vuksanović, Lj. M. Totovski, R. M. Jančić Heinmann, D. Ž. Mijin, Sci. Sinter., 53 (2021) 91-117.
23.   M. S. Manzar, A. Waheed, I. W. Qazi, N. I. Blaisi, N. Ullah, J. Taiwan Inst. Chem. Eng., 97 (2019) 424-432.

_____

Сажетак: *Нови магнетични полимер/бентонит композит је припремљен суспензионом кополимеризацијом глицидил-метакрилата и етилен гликол диметакрилата у присуству магнетичног бентонита (MB-PGME) и функционализован етилен диамином (MB-PGME-ED) и хексаметилен диамином (МБ-ПГМЕ-ХД). Добијени узорци су окарактерисани у погледу структуре, као и термичких, магнетних и морфолошких својстава. Испитивана је сорпција ренијума (Re) и волфрама (W) из воденог раствора на MB-PGME-ED и MB-PGME-HD узимајући у обзир њихово време контакта и различите почетне концентрације јона, што даје могућност употребе ових полимера као комерцијалних сорбената. Сорпциони систем прати кинетик псеудо-другог реда уз утицај дифузије унутар честица. Резултати су показали најбоље слагање са Фројндлиховим моделом изотерме.*
Кључне речи*: глицидил метакрилат, магнетични бентонит, амино-функционализација, сорпција.*